

Effect of Solenoidal Magnetic Field on Time Evolution of Ion Beam Emittance in Laser Ion Source^{*)}

Hiroto KATANE, Kakeru MIYAZAKI, Kaoru ISHIKURO, Naoto HARUKAWA,
Kazumasa TAKAHASHI, Toru SASAKI and Takashi KIKUCHI

Nagaoka University of Technology, Nagaoka, Niigata 940-2188, Japan

(Received 10 January 2022 / Accepted 7 April 2022)

Applying a solenoidal magnetic field to a laser ion source is a method to produce a high current beam. In this study, we measured the effect of the solenoidal magnetic field on the time evolution of the ion beam emittance using the double-slit method for the laser ion source. Ablation plasma was produced by irradiating an Al target with an Nd:YAG laser. From the emittance measurements, the phase difference shown in the time evolution of the emittance ellipses increased as the ion current increased by applying a magnetic field. In addition, the emittance increased with increasing time range for the averaged current in the waveform. However, the emittance using the averaged current in a pulse was almost constant with the magnetic field. These results indicate that the brightness of the beam increased as the ion beam current increased using the solenoidal magnetic field.

© 2022 The Japan Society of Plasma Science and Nuclear Fusion Research

Keywords: emittance, beam brightness, ion beam, laser ion source, double-slit method, heavy-ion inertial fusion, solenoidal magnetic field

DOI: 10.1585/pfr.17.2404067

1. Introduction

Heavy-ion inertial fusion (HIF) requires high current beams of the order of 100 kA on a fuel target for nuclear fusion. However, the Child-Langmuir law limits the beam current, and an ion beam with a large current cannot be accelerated. Therefore, many HIF scenarios suggest that beams with a current lower than the space-charge-limited current derived by the law are produced by extracting ion beams from multiple ion sources. Then, the beams are merged and bunched during acceleration and transported to ensure that the large beam current satisfies the requirement at the final focus [1–4]. The ion source for HIF requires a beam current of 0.5 A or more and a normalized emittance of $1 \pi \text{ mm mrad}$ or less when using induction accelerators [5, 6]. The emittance is defined by the particle distribution in the space and momentum coordinates and indicates the beam quality in the two-dimensional phase space.

A laser ion source can supply a high current pulse beam and is proposed to provide an ion current that satisfies these requirements. In addition, the beam current can be enhanced by applying a solenoidal magnetic field to the laser ion source [7–9]. However, the effect of the solenoidal magnetic field on beam emittance has not been clarified. In general, an ablation plasma generated by laser irradiation has a shifted Maxwellian velocity distribution, which indicates a variation in plasma density over time in the pulse. Consequently, the plasma meniscus, which is the

surface of ion extraction from the plasma, can be changed owing to the change in plasma density, which can cause rotation of the phase of the emittance ellipse [10]. Therefore, the emittance for the entire beam pulse may increase when the current is increased by applying the solenoidal magnetic field because the phase variation of the emittance ellipse increases.

Beam brightness is also one of the indicators of ion beam characteristics and is expressed using emittance ε and ion beam current I as follows:

$$B = 2I/\pi^2 \varepsilon^2 [\text{A}/(\text{mm mrad})^2]. \quad (1)$$

The increase in beam emittance can reduce the brightness, whereas HIF requires high-brightness beams. In this study, the effect of the solenoidal magnetic field on the time evolution of the RMS (root mean square) emittance of the ion beam generated from the laser ion source is investigated, and the variation in the emittance of the entire pulse and beam brightness is discussed.

2. Emittance Measurement Method

We used the double-slit method for the emittance measurements. By scanning two slits throughout the beam area, the beam distribution in the transverse phase space can be obtained. The RMS emittance of the ion beam ε_{rms} was calculated from the phase-space distribution of the beam current I obtained at each position and angle as follows:

$$\varepsilon_{\text{rms}} = \sqrt{\langle x^2 \rangle \langle x'^2 \rangle - \langle xx' \rangle^2} [\pi \text{ mm mrad}], \quad (2)$$

author's e-mail: hkatane@stm.nagaokaut.ac.jp

^{*)} This article is based on the presentation at the 30th International Toki Conference on Plasma and Fusion Research (ITC30).

$$\begin{aligned}\langle x^2 \rangle &= \iint x^2 I(x, x') dx dx' / \iint I(x, x') dx dx', \\ \langle x'^2 \rangle &= \iint x'^2 I(x, x') dx dx' / \iint I(x, x') dx dx', \\ \langle xx' \rangle &= \iint xx' I(x, x') dx dx' / \iint I(x, x') dx dx'.\end{aligned}\quad (3)$$

In general, the phase-space distribution of the RMS beam emittance is elliptical. To clarify the variation in the beam convergence, we compared the slopes of the ellipses. The ellipse can be drawn using Twiss α , β , γ parameters derived using Eqs. (4) and (5).

$$\gamma x^2 + 2\alpha xx' + \beta x'^2 = \varepsilon_{\text{rms}}, \quad (4)$$

$$\begin{aligned}\gamma &= \sqrt{\langle x^2 \rangle} / \varepsilon_{\text{rms}}, \\ \beta &= \sqrt{\langle x'^2 \rangle} / \varepsilon_{\text{rms}}, \\ \alpha &= \pm \sqrt{1 + \beta\gamma}.\end{aligned}\quad (5)$$

3. Experimental Setup

The experimental setup is shown in Fig. 1. The ablation plasma was produced by irradiating an Al target with an Nd:YAG laser. The laser intensity at the target was 1.5×10^{10} W/cm². The pressure in the chamber was maintained at approximately 5×10^{-3} Pa throughout the experiment.

A magnetic field for increasing the plasma ion flux was generated using a solenoidal coil with a diameter of 55 mm, width of 30 mm, and 320 turns. The coil can produce a magnetic flux density of 5.5 mT per 1 A of coil current at the center of the coil. The distance from the target to the solenoidal coil was 350 mm, and the distance from the target to the ion extraction electrode was 950 mm.

Ion beam extraction from the plasma was performed using three electrodes, which allowed control of the plasma meniscus of the ion extraction surface while maintaining constant accelerated ion energy. The diameters of the first, second, and third electrodes were 3 mm, 5 mm, and 7 mm, respectively. The gaps between the electrodes were both 10 mm. The biased voltages at the first, second, and third electrodes were 13 kV, 10.5 kV, and 0 V (GND), respectively. The voltages of the first and second electrodes were determined to prevent breakdown between the electrodes

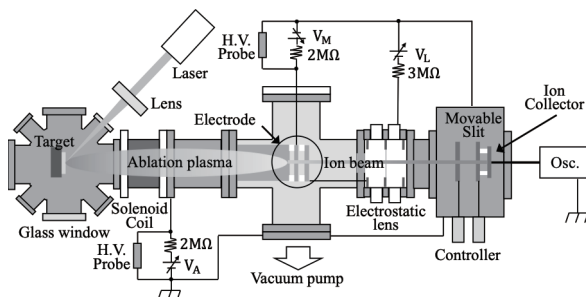


Fig. 1 Experimental system.

and achieve the highest current in the center of the beam axis at the ion collector position.

The ion beam diameter was controlled at approximately 10 mm at the position of the double slit using an electrostatic lens. An electrostatic lens composed of three electrodes was designed based on the simulation results obtained using beam simulation software, IGUN. The diameters of the first and third electrodes were 70 mm, and the distance from the second electrode was 30 mm in both gaps. The second consisted of a stainless-steel mesh with a transmittance of 71%. The potentials of the first and third electrodes were grounded, and the second electrode was biased at -7 kV.

The beam diameter and angular distribution were scanned using a double slit. The beam-scanning system was composed of two slits and an ion collector. The widths of the first and second slits were 1 mm and 0.5 mm, respectively, and the distance between them was 46 mm. We scanned the first and second slits at 1 mm and 0.5 mm intervals, respectively. The ion collector was placed behind the second slit, with a gap of 10 mm between them.

4. Results and Discussion

Figure 2 shows the variation in the peak of the ion beam current waveform as a function of the solenoidal magnetic field. The measurement was performed with only the second slit placed at the center of the beam axis. From this result, the current started to drastically increase at approximately 2.2 mT and reached the maximum at 3.3 mT, gradually decreased after 3.3 mT. Thus, the emittances were measured at four magnetic flux densities: (a) 0.0 mT, (b) 2.5 mT, (c) 3.3 mT, and (d) 7.7 mT. The waveforms of the ion beam current with the magnetic fields are shown in Fig. 3. A time of 0 s indicates the timing of laser irradiation on the target.

To investigate the effect of the variation in the ion current density on the plasma meniscus, the ion current densities at the ion extraction point were compared to the space-charge-limited current density calculated using the Child-Langmuir law. Laser ablation plasmas have a drift veloc-

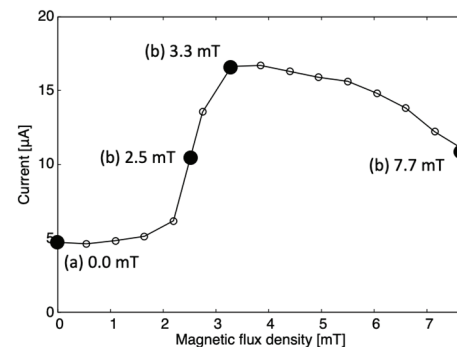


Fig. 2 Peak of ion beam current as a function of the solenoidal magnetic field.

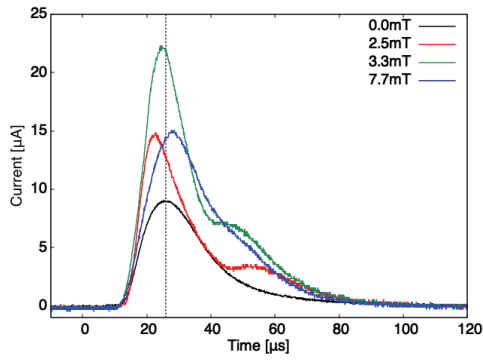


Fig. 3 Waveforms of ion beam current with solenoidal magnetic fields of 0.0 - 7.7 mT.

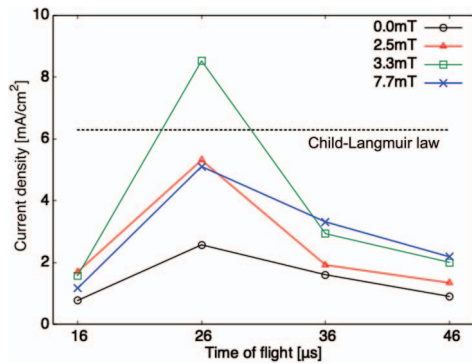


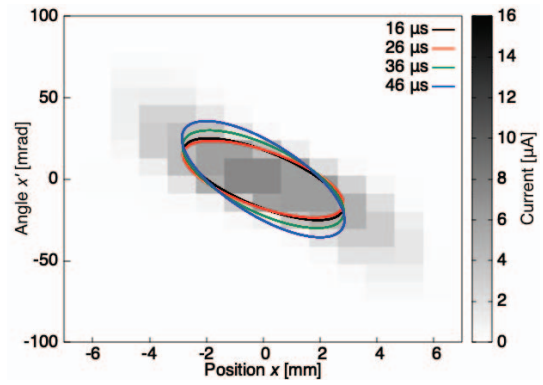
Fig. 4 Time evolution of the ion current density with the solenoidal magnetic field.

ity; therefore, the space-charge-limited current density was calculated using the following equation [11]:

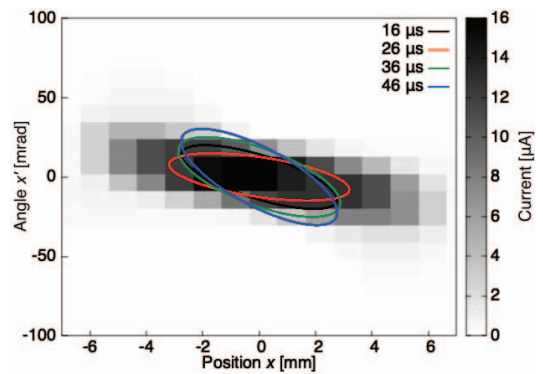
$$J_{CL} = \frac{4}{9} \epsilon_0 \sqrt{\frac{2Ze}{m_i}} \frac{(\sqrt{V_0} + \sqrt{V_0 + V_a})^3}{d^2}, \quad (6)$$

where ϵ_0 , Z , e , m_i , and d are the vacuum permittivity, ion-charge state, elementary charge, ion mass, and gap distance of the electrode for acceleration, respectively. Voltages V_a and V_0 are the acceleration voltage and voltage corresponding to the kinetic energy of ions ZeV_0 in the plasma, respectively. Figure 4 shows that the variation in the ion current density increased with the solenoidal magnetic field, implying that the variation in the plasma meniscus increased accordingly.

Figure 5 shows the phase-space distributions with and without the magnetic field obtained using the averaged current in the range of 16 - 36 μ s. The duration was determined based on the result that the peak of the current waveforms was obtained at approximately 26 μ s, and the pulse duration of the full width at half maximum was approximately 20 μ s, as shown in Fig. 3. In addition, the emittance ellipses calculated at 16 - 46 μ s with 10 μ s intervals are shown to clarify the time evolution of the phase in the ellipse. As shown in Fig. 5, the slope of the phase-space distribution at 3.3 mT was slightly smaller than that at 0.0 mT. Moreover, the variation in the slope of the ellipse



(a) Phase-space distribution at 0.0 mT.



(b) Phase-space distribution at 3.3 mT.

Fig. 5 Phase-space distributions and emittance time evolution with and without the solenoidal magnetic field. The maps are drawn with averaged current in the range of 16 - 36 μ s.

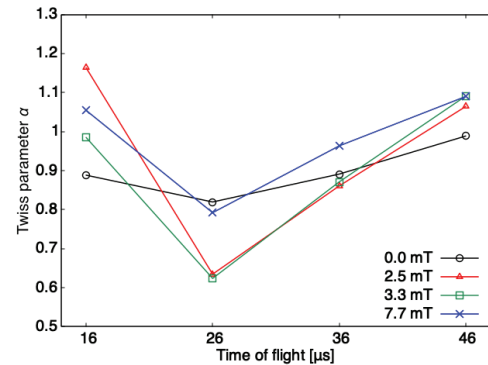


Fig. 6 Time evolution of Twiss parameter α .

during time evolution with the magnetic field was larger than that without the magnetic field.

To evaluate the variation in the slope of the ellipse, the Twiss parameter α was compared because it represents beam convergence and corresponds to the slope of the emittance ellipse. Figure 6 shows the time evolution of the Twiss parameter α for different magnetic fields. This result indicates that the difference in the time evolution of the emittance increases with an increase in the ion beam current. This can be explained by the change in the meniscus

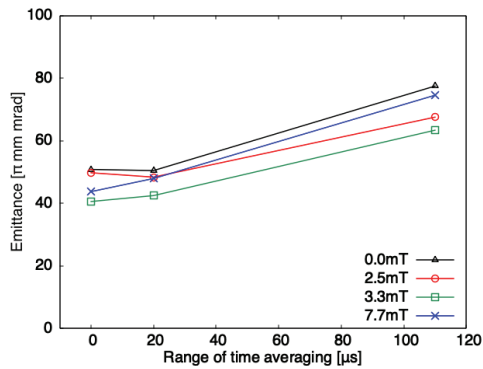


Fig. 7 Emittance variation as a function of the time range for the averaged current in the waveform.

cus of the ion extraction surface. When a magnetic field was applied to the plasma, the plasma density at the ion extraction position was higher than that without the magnetic field. As the plasma density increases, the ion extraction surface expands to the ion extraction gap and the beam divergence increases [3]. Since the focusing force of the electrostatic lens was constant, the convergence angle of the ion beam decreased at the double slit because of the increase in plasma density with the magnetic field.

In addition, to investigate the influence of the variation in the emittance time evolution on the emittance for the entire pulse, we calculated the emittance at several time ranges for the averaged current in the waveforms (a) 26 μs , (b) 16–36 μs and (c) 10–120 μs for each magnetic field condition. As shown in Fig. 7, the emittance increased with an increase in the range of time averaging. Conversely, the emittance variation did not increase by applying a magnetic field despite the increase in the variation of α .

Figure 8 shows the emittance obtained using the averaged current 16–36 μs at and the beam brightness calculated using the emittance as a function of the magnetic field. The emittance was almost constant though the beam current increased markedly by solenoidal magnetic field. As the result of emittance variation, the beam brightness varied, similar to the ion current variation, by applying a magnetic field; therefore, the brightness of the beam could be increased with the increase in the ion beam current.

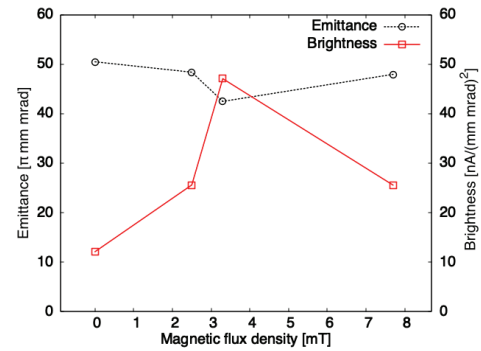


Fig. 8 Beam brightness and the emittances obtained using the averaged current at 16–36 μs as a function of the magnetic field.

5. Conclusion

This study aimed to clarify the effect of the solenoidal magnetic field on the time evolution of the ion beam emittance and the brightness of the laser ion source. Based on the emittance measurements with several solenoidal magnetic flux densities, the phase difference shown in the time evolution of the emittance ellipse increased as the ion current increased by applying a solenoidal magnetic field. In addition, the emittance increased with increasing time range for the averaged current in the waveform. On the other hand, the emittance obtained using the averaged current at 16–36 μs was almost constant with the magnetic field. Thus, the beam brightness increased as the ion beam current increased using the solenoidal magnetic field.

- [1] R.O. Bangerter, A. Faltens and P.A. Seidl, *Rev. Accel. Sci. Tech.* **6**, 85 (2013).
- [2] I. Hofmann, *Matter Radiat. Extremes* **3**, 1 (2018).
- [3] K. Horioka, *Matter Radiat. Extremes* **3**, 12 (2018).
- [4] K. Takayama *et al.*, *Phys. Lett. A* **384**, 126692 (2020).
- [5] J.W. Kwan *et al.*, *Nucl. Instrum. Meth. Phys. Res. A* **464**, 379 (2001).
- [6] J.W. Kwan, *IEEE Trans. Plasma Sci.* **33**, 1901 (2005).
- [7] M. Okamura *et al.*, *Rev. Sci. Instrum.* **81**, 02A510 (2010).
- [8] T. Kanesue *et al.*, *Appl. Phys. Lett.* **105**, 193506 (2014).
- [9] M. Okamura *et al.*, *Nucl. Instrum. Methods Phys. Res. A* **733**, 97 (2014).
- [10] M. Sekine *et al.*, *Nucl. Instrum. Methods Phys. Res. A* **795**, 151 (2015).
- [11] H. Riege, *Nucl. Instrum. Methods Phys. Res. A* **451**, 394 (2000).